9) as a photosensitizer. As briefly reported,[2c] the photoreaction proceeding via reductive quenching (mechanism I) gives a higher quantum yield as compared with that initiated by oxidative quenching of the excited RuL_3^{2+} by MV^{2+} (mechanism II), in which the unfavorable back electron transfer from MV^+ to RuL_3^{3+} reduces the overall quantum yield. Data in Table V are in good support for the present argument. Namely, the high quantum yields were attained only when mechanism I prevails.

mechanism I (reductive quenching):

$$*RuL_3^{2+} + TEA \rightarrow RuL_3^{+} + TEA^{ox} \not\leftarrow RuL_3^{2+} + TEA$$

$$RuL_3^{+} + MV^{2+} \rightarrow RuL_3^{2+} + MV^{+}$$

mechanism II (oxidative quenching):

$$*RuL_3^{2+} + MV^{2+} \rightarrow RuL_3^{3+} + MV^{+} \rightarrow RuL_3^{2+} + MV^{2+}$$

$$RuL_3^{3+} + TEA \rightarrow RuL_3^{2+} + TEA^{ox}$$

For Ru(2,2′-bipyrazine)$_3^{2+}$ (L = **8**), the quantum yield of 1.7 needs to be explained. In an alkaline medium or at a high TEA concentration as in the present case, the TEA cation radical produced by electron transfer is known to release a proton[44] and the resulting TEA radical is able to reduce another MV^{2+}. In a high-pH region, the overall reaction can be thus expressed as eq 6. Analogous features are observed for Ru(2,2′-bipyrimidine)$_3^{2+}$ in aqueous solution as well ([Ru(2,2′-bipyrimidine)$_3^{2+}$] = 6×10^{-5} M, [MV^{2+}] = 0.02 M, [TEA] = 0.5–1.2 M).[12] In this case, ϕ_{MV^+} increases with the increase in [TEA] and the limiting ϕ_{MV^+} at infinite TEA concentration was 1.56. In a high pH region or at a high TEA concentration, participation of the reactions in eq 4 and 5 cannot be eliminated for all reaction systems examined in this study.

$$*RuL_3^{2+} + TEA \rightarrow RuL_3^{+} + TEA^{ox}(R_2N^{\cdot+}CH_2CH_2OH) \quad (2)$$

$$RuL_3^{+} + MV^{2+} \rightarrow RuL_3^{2+} + MV^{+} \quad (3)$$

$$R_2N^{\cdot+}CH_2CH_2OH \rightleftharpoons R_2NCH_2\dot{C}HOH + H^+ \quad (4)$$

$$R_2NCH_2\dot{C}HOH + MV^{2+} \rightarrow R_2NCH_2CHO + MV^{+} + H^+ \quad (5)$$

$$\text{net: } RuL_3^{2+} + 2MV^{2+} \xrightarrow[TEA]{h\nu} RuL_3^{2+} + 2MV^{+} \quad (6)$$

(44) Kalyanasundaram, K.; Kiwi, J.; Graetzel, M. *Helv. Chim. Acta* **1978**, *61*, 2720.

Conclusions

To develop efficient redox photosensitizers, it is obvious that Ru(bpy)$_3^{2+}$ is not the best among its analogues. On the basis of the present study, modulation of the π-accepting ($E_{1/2}(L/L^-)$) and σ-donating abilities (pK_a) of L is a plausible approach for efficient photoredox systems. For photoreduction of MV^{2+} in the RuL_3^{2+}–MV^{2+}–TEA systems, RuL_3^{2+} complexes having a ground-state reduction potential more positive than −1.2 V are subjected to reductive quenching by TEA and will act as more efficient photosensitizers than Ru(bpy)$_3^{2+}$.

RuL_3^{2+} species (L = **5**, **6**, **9**) possessing a lower ^{3}MLCT* state energy relative to that of Ru(bpy)$_3^{2+}$ showed a smaller temperature dependence of τ (<1000 cm^{-1}). The lowering of the emitting ^{3}MLCT* state energy, however, leads in general to a decrease in the excited-state lifetime (i.e., energy gap law). Among 12 RuL_3^{2+} complexes, only Ru(3,3′-bipyridazine)$_3^2$ (L = **9**) exhibits a small temperature dependence of τ as well as a relatively long emission lifetime (1050 ns at 298 K). Also, this complex shows strong reduction and oxidation abilities and an absorption energy comparable with that of Ru(bpy)$_3^{2+}$. Ru(3,3′-bipyridazine)$_3^{2+}$ certainly has more advantages than Ru(bpy)$_3^{2+}$ as a photoredox sensitizer.

Acknowledgment. We are greatly indebted to H.-B. Kim and M. Sato for their collaboration in lifetime measurements and photodecomposition experiments, respectively. This work was partly supported by a Grant-in-Aid for Special Study from the Ministry of Education, Science and Culture of Japan (No. 61040046).

Contribution from the University Chemical Laboratory, University of Cambridge, Lensfield Road, Cambridge CB2 1EW, England

Intensity Distributions within the "d–d" Spectra of Tetrakis(diphenylmethylarsine oxide)(nitrato)cobalt(II) and Tetrakis(diphenylmethylarsine oxide)(nitrato)nickel(II) Nitrates†

Neil D. Fenton and Malcolm Gerloch*

Received August 4, 1988

The relative intensities of the polarized "d–d" transitions of the title complexes have been reproduced quantitatively within a new ligand-field scheme. The model is parametrized by quantities that relate to the electron densities within the individual metal–ligand bonds. General chemical bonding principles that characterize conventional ligand-field analysis are used to interpret the parameter values of the present intensity analyses. Descriptions of the detailed nature of the coordination in the complexes arising from this intensity study agree in detail with those deriving from earlier ligand-field analyses of transition energies, paramagnetic susceptibilities, and ESR g values.

Introduction

The data base of ligand-field analysis for transition-metal and lanthanide complexes has traditionally comprised spectral transition energies together with paramagnetic susceptibilities and ESR g values. The sophistication of modern ligand-field analysis is such that we now expect to reproduce each of these properties, quantitatively within experimental error, for all mononuclear higher oxidation state (Werner-type) transition-metal complexes, regardless of coordination number, molecular geometry or symmetry, or of d^n or f^n configuration.[1] The greatest chemical transparency attaches to those ligand-field models with parameters that refer to local bonding features in molecules. The cellular ligand-field (CLF) model, like the molecular-orbital-based scheme of the angular overlap model (AOM) that preceded it, employs separate parameters for each ligand and for each local bonding mode (σ, π_x, π_y). The age-old chemical notion of the functional group is thus built into the best modern ligand-field schemes from the beginning.[1-4] It is just these structural features that endow

† No reprints are available from this laboratory.

(1) Gerloch, M. *Magnetism and Ligand-Field Analysis*; Cambridge University Press: Cambridge, England, 1983.

0020-1669/89/1328-2975$01.50/0 © 1989 American Chemical Society

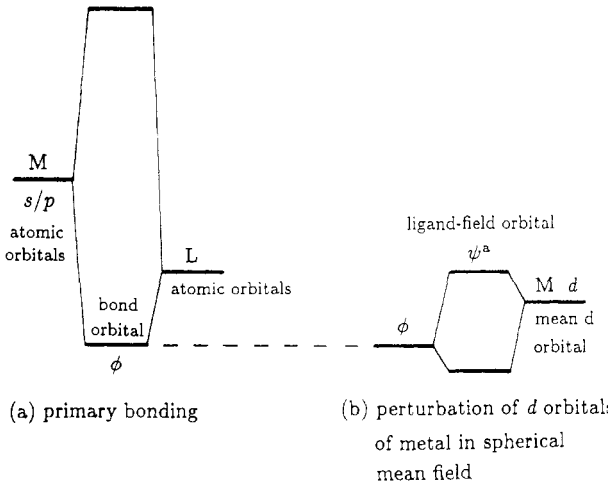

Figure 1. Ligand field in a transition-metal complex viewed in part b as a perturbation on the primary metal–ligand bonding in part a.

current ligand-field analyses with their ability to reflect, immediately and within mainstream chemical vocabulary, the way the d (or f) orbitals probe the underlying bonding electron density. We consider this cellular structure to be a sine qua non of any contemporary ligand-field model for which is claimed more than mere statements of gross molecular point-group symmetry.

One easily measurable ligand-field property has almost universally been omitted from ligand-field analysis. The intensities or even the intensity distributions (meaning relative intensities) within "d–d" or "f–f" spectral transitions have long been considered to be outside the scope of ligand-field theory. At a qualitative level in teaching courses, we refer to spin and orbital selection rules, to the sharpness of some spin-forbidden transitions ("spin–flip"), to the weakness of some spin-allowed bands ("two-electron jumps"), or to such gross features of polarization ratios as derive from the exercise of the direct product. We do not address the quantitative question of why one band is, e.g., 43 times as intense as another and 105 times less intense than a third. While not generally part of ligand-field analysis, as such, there have been, however, a number of quantitative studies of these spectral intensities, mostly deriving from the work of Judd[5-7] and of Ofelt.[8] Like Judd's work, subsequent developments by Mason,[9] by Newman,[10] and especially by Richardson[11-14] have focused mostly upon lanthanide f^n spectra. At the phenomenological level, their latest studies have met with considerable success. Rather less work has been reported on the intensities of d^n spectra. While Newman's[10] and, later, Richardson's and Reid's studies[12,14] have employed the principle of spatial superposition, the parametrization of a cellular model able to separate interactions in the same way as earlier ligand-field studies of energies has only recently been attempted.[16-18]

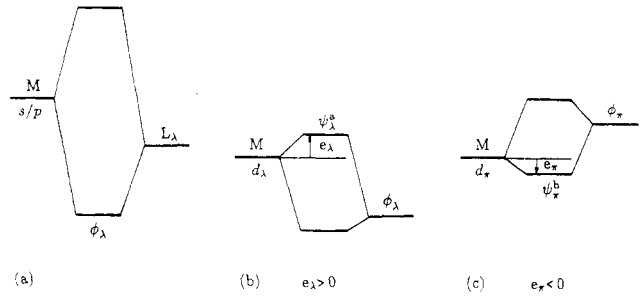

Figure 2. Definitions of ligand-field parameters referring to one local cell. Primary bonding (a) defines the local bond orbital, and subsequent energy shifts of appropriately matched d orbitals define cellular ligand-field parameters (b) for ligand donors, or (c) for ligand π acceptors.

Elsewhere,[16] we describe a modeling of "d–d" (and, in principle, "f–f") intensity distributions arising from the static environment in acentric chromophores that considers these data as properties on a par with magnetic susceptibilities insofar as their computation within a ligand-field analysis is concerned. Here, we summarize its parametric structure against a background of the theory of ligand fields.

Ligand-field theory is concerned with manipulations of matrix elements of pure d (f) functions under the operators of interelectron repulsion, the effective ligand-field potential, and spin–orbit coupling. It does not deal *directly* with the chemical bonding in a complex. A useful pictorial summary[19] of the ligand-field approach is provided by the scheme in Figure 1. Here, we imagine the primary step of bond formation between the valence orbitals of metal and ligands. In higher oxidation state complexes at least, the contribution of metal d orbitals to the valence shell is minimal as they are radially so compact. It is then a good approximation, as represented in the figure, to consider the effect of the bonding orbitals so formed upon the d orbitals as a secondary perturbation. Now, as a result of the electron redistribution that occurs in forming a complete complex from metal and ligands, in response to the electroneutrality principle and all else that is part of "bonding", the d orbitals to be used as the ligand-field basis span the mean, spherical part of the molecular Hamiltonian rather than that of the free metal atom or ion. We refer to them as the mean d orbitals of the complex. Their radial character is unknown to us and will vary from system to system. Similarly, sufficiently exact forms of the bonding orbitals in the complex are beyond guessing. So their joint contributions are subsumed within the usual ligand-field parameters, $\langle d|V_{LF}|d\rangle$. These variables therefore monitor, or probe, aspects of the character of both d and bond orbitals in the complex under study.

The corresponding view within the *local* spatial region associated with any one M–L ligation—a cell—is sketched in Figure 2. Contributions to the energy shifts of the mean d orbitals are parameterized by reference to the local σ and π bonding with the cellular ligand-field parameters, e_σ and e_π. In normal ligand-field analysis no further reference is made to the ligand-field orbitals (or, within the local frame, the cellular orbitals, ψ) except in an averaged way through orbital reduction factors in the computation of magnetic properties. The small departures from pure d character in the cellular orbitals are of the essence, however, for an investigation of spectral intensities. The non-d character of the cellular orbitals will comprise both metal s and p functions together with appropriate (symmetry-matched) ligand functions: e.g. for σ orbitals

$$\psi_\sigma \sim d_\sigma^M + c_1 s^M + c_2 p_\sigma^M + c_3 \phi_\sigma^L \qquad (1)$$

where the c values are small mixing coefficients. Those functions referred to the ligand as center (as indicated by the superscript) can be replaced by a combination of multipoles centered on the metal. It is unimportant for present purposes to specify the precise

(2) Gerloch, M.; Woolley, R. G. *Prog. Inorg. Chem.* **1984**, *31*, 371.
(3) Woolley, R. G. *Int. Rev. Phys. Chem.* **1987**, *6*, 93.
(4) Gerloch, M. In *Understanding Molecular Properties*; Avery, J. S., Dahl, J. P., Hansen, A., Eds.; Reidel: Amsterdam, 1987; p 111.
(5) Judd, B. R. *Phys. Rev.* **1962**, *127*, 750.
(6) Judd, B. R. *J. Chem. Phys.* **1979**, *70*, 4830.
(7) Jørgensen, C. K.; Judd, B. R. *Mol. Phys.* **1964**, *8*, 281.
(8) Ofelt, G. S. *J. Chem. Phys.* **1962**, *37*, 511.
(9) Mason, S. F.; Peacock, R. D.; Stewart, B. *Mol. Phys.* **1975**, *30*, 1829.
(10) Poon, Y. M.; Newman, D. J. *J. Phys. Chem.* **1984**, *17*, 4319.
(11) Richardson, F. S. *Chem. Phys. Lett.* **1982**, *86*, 47.
(12) Reid, M. F.; Richardson, F. S. *J. Chem. Phys.* **1983**, *79*, 5735.
(13) Reid, M. F.; Richardson, F. S. *J. Phys. Chem.* **1984**, *88*, 3579.
(14) Reid, M. F. *J. Chem. Phys.* **1987**, *87*, 6388.
(15) Reid, M. F.; Dallara, J. J.; Richardson, F. S. *J. Chem. Phys.* **1983**, *79*, 5743.
(16) Brown, C. A.; Gerloch, M.; McMeeking, R. F. *Mol. Phys.* **1988**, *64*, 771.
(17) Brown, C. A.; Duer, M. J.; Gerloch, M.; McMeeking, R. F. *Mol. Phys.* **1988**, *64*, 793.
(18) Brown, C. A.; Duer, M. J.; Gerloch, M.; McMeeking, R. F. *Mol. Phys.* **1988**, *64*, 825.
(19) Gerloch, M. Submitted for publication in *Coord. Chem. Rev.*

Table I. Parametric Structures of the Cellular Ligand-Field Model

CLF energy parameters	CLF transition-moment parameters
e_σ	${}^{P}t_\sigma$, ${}^{F}t_\sigma$, ${}^{R}t_\sigma$
$e_{\pi x}$	${}^{P}t_{\pi x}$, ${}^{F}t_{\pi x}$, ${}^{R}t_{\pi x}$
$e_{\pi y}$	${}^{P}t_{\pi y}$, ${}^{F}t_{\pi y}$, ${}^{R}t_{\pi y}$

details, or notation, of such an expansion (see, for example, Sharma[20]): we just write

$$\phi_\sigma{}^{L} = a_1 s^{M} + a_2 p_\sigma{}^{M} + a_3 d_\sigma{}^{M} + a_4 f_\sigma{}^{M} + \ldots \quad (2)$$

and observe, anthropomorphically, that the ligand function appears to the metal as a sum of s, p, d, ... metal functions. The cellular orbitals of (1) then become

$$\psi_\sigma \sim d_\sigma{}^{M} + b_1 s^{M} + b_2 p_\sigma{}^{M} + b_3 f_\sigma{}^{M} + \ldots \quad (3)$$

Now, the computation of "d–d" intensities recognizes the predominance of the electric-dipole contribution. Writing cellular orbitals generally as

$$\psi \sim d + b\chi \quad (4)$$

where χ represents all non-d functions, admixed by *any* means, orbital transition moments, **Q**, take the form

$$\mathbf{Q} = \langle\psi|er|\psi\rangle \quad (5)$$

$$= \langle d|er|d\rangle \quad (6a)$$

$$+ 2b\langle d|er|\chi\rangle \quad (6b)$$

$$+ b^2\langle\chi|er|\chi\rangle \quad (6c)$$

The usual selection rule for electric dipole transitions, $\Delta l = \pm 1$, means that the first contribution (6a) vanishes always and that the term (6b) survives only for those parts of χ transforming as p or f with respect to the metal center. We will discuss the third term (6c) shortly.

We write nonzero contributions from (6b) as *parameters* ${}^{L}t_\lambda$ of the system:

$$\left.\begin{aligned} {}^{P}t_\lambda &= b_p\langle d|ez|p\rangle \\ {}^{F}t_\lambda &= b_f\langle d|ez|f\rangle \end{aligned}\right\}_{\lambda=\sigma,\pi_x,\pi_y} \quad (7),\ (8)$$

where the coefficients b_p and b_f subsume all earlier coefficients arising from the description of the bond orbitals in (1) and of the multipole expansion in (2). For all the reasons given above, we make no attempt to calculate such coefficients—or the radial forms of d and p/f basis functions—considering as ever that the ligand-field model should be excused the tasks of bonding theory. The parametrization scheme outlined here merely implants the bonding and cellular structure, so effective elsewhere in ligand-field theory, into the core of the intensity procedures. Interpretations of the ${}^{L}t_\lambda$ parameters are then made by reference to the same qualitative chemical concepts that characterize successful ligand-field analyses of transition energies and magnetic properties.

The third contribution (c) to the transition moment in (6) cannot be discarded simply on the grounds that for $b \ll 1$, b^2 is negligible. For while the integrals $\langle d|er|p\rangle$ and $\langle d|er|f\rangle$ are on the order of 0.1 au at most, $\langle\chi|ez|\chi\rangle$ (z parallel to the M–L vector) is simply equal to an effective bond length and so perhaps is 10–20 times larger.[18] Special circumstances of molecular geometry, however, conspire to reduce the significance of this third contribution in many cases and that is one issue we address in the present study. For the moment, we define the parameters

$${}^{R}t_\lambda = b^2\langle\chi|ez|\chi\rangle \quad (9)$$

the last part of (6).

Altogether, therefore, our model is parameterized at the orbital level by the local quantities ${}^{L}t_\lambda$ ($L = P, F, R$; $\lambda = \sigma, \pi_x, \pi_y$) in much the same way that the local energy shifts are parameterized by e_λ; all this is summarized in Table I. Ultimately, the implementation of the present model for intensity distributions is carried out within the same general structure as for the calculation of other ligand-field properties. Although e_λ and ${}^{L}t_\lambda$ parameters could be optimized together, it has proved to be totally satisfactory to base intensity analyses upon prior ligand-field analyses of all other properties.[17] The same procedure is followed in the present study.

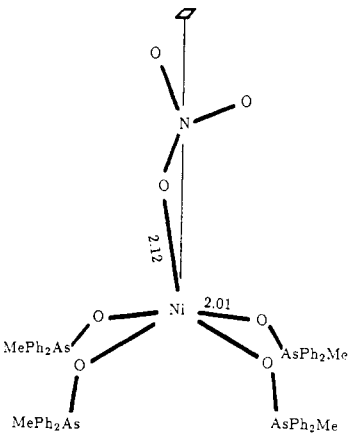

Figure 3. Coordination geometry in $[Ni(OAsPh_2Me)_4NO_3]^+$. The nitrates are disordered in the tetragonal lattice.[25]

The chemical significance of this new approach centers upon the interpretations of the ${}^{L}t_\lambda$ parameter values. In the earlier study,[17,18] spectra of some 13 four- and five-coordinate, noncentric complexes were reproduced quantitatively, and some preliminary ideas about the chemical relevance of the parameters were formed. We test the model further in the present paper, not only to observe its quantitative reproduction of experimental data but also to see if the earlier views continue to receive support. Not least of these is that understanding of the electron distribution within the bonding of the complex, which derived from study of the more traditional ligand-field properties, consistently matches that suggested by the intensity analysis also.

It is obvious from Table I that the intensity model is very highly parametrized. Nevertheless, experience to date has shown that unique fits to experimental intensities and polarization ratios are usually possible, and indeed, the analyses proceed rather more smoothly than the corresponding ligand-field analyses of energies with the smaller $\{e\}$ parameter sets. In part this has been due to the unimportance in the earlier analyses of the ${}^{R}t_\lambda$ parameters. As discussed elsewhere,[16] only those contributions to $\{{}^{R}t_\lambda\}$ for the light vector parallel to the local bond vector are retained in the parameterization scheme. For the remaining components, it is simple to show[18] that their overall contribution when summed over all ligands in a complex will cancel for bipyramids and antiprisms (skewed or not). The intensity parameter sets for the earlier analyses[17,18] of tetrahedra and trigonal bipyramids, therefore, were reduced to the ${}^{P}t_\lambda$ and ${}^{F}t_\lambda$ subsets. That residual "double layer" of parameters—relative to the single set of e_λ required in the prior ligand-field analysis—turns out to be particularly revealing of the underlying electron distribution in the complex. Thus, in addition to the obvious enquiry into the relative magnitudes and signs of the σ and π type parameters and their relation to the corresponding e_λ variables, the observed ratios ${}^{P}t_\lambda{:}{}^{F}t_\lambda$ provide commentary upon the variation in bond polarity throughout a series of chromophores. The sensitivity of calculated intensity distributions to the ratios of P and F type contributions is quite marked. Altogether, inclusion of intensity data into ligand-field analyses promises to enhance greatly our ability to comment on bonding electron density distributions.

In the present study, we investigate the single-crystal polarized spectra[21,22] of two square-based pyramidal chromophores that have

(20) Sharma, R. R. *Phys. Rev. A* **1976**, *13*, 517.

(21) Gerloch, M.; Kohl, J.; Lewis, J.; Urland, W. *J. Chem. Soc. A* **1970**, 3269.

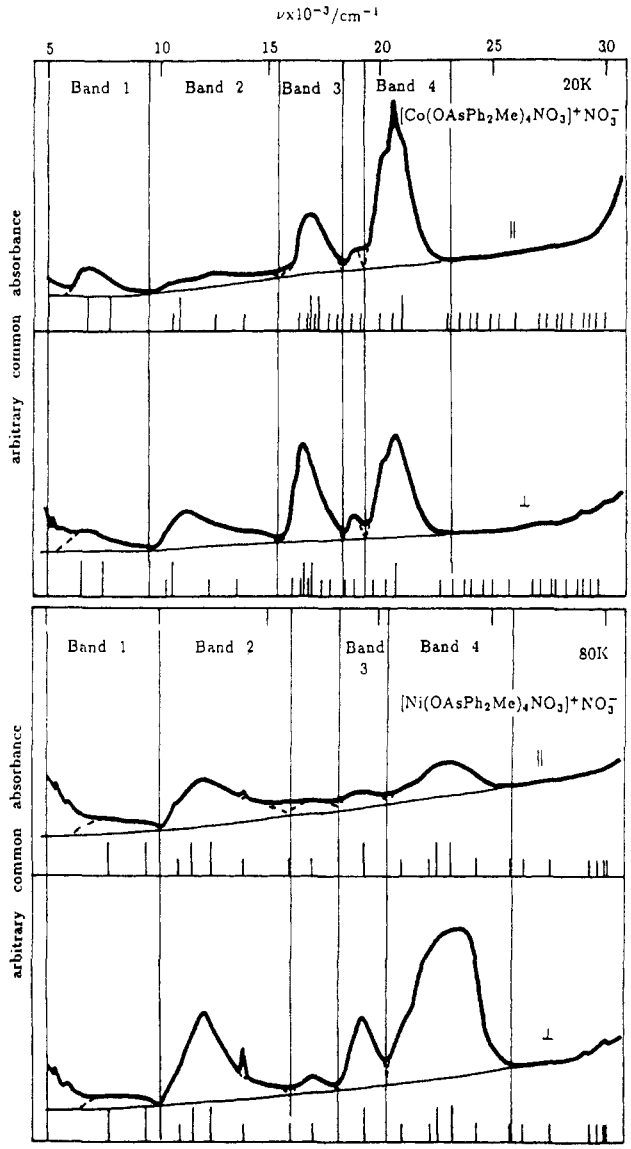

Figure 4. Polarized spectra of $[M(OAsPh_2Me)_4NO_3]^+NO_3^-$ (M = Co(II), Ni(II)). Calculated transition energies[23] are shown by long and short markers for spin-allowed and spin-forbidden transitions. Integrated absorbances of transitions falling within the bounds of the indicated "bands" were used in the intensity analysis. Separate commentary on the resolvable spin-forbidden bands is made in the text.

been the subject of very detailed ligand-field analysis[23] with respect to transition energies, paramagnetic susceptibilities[21,22] and ESR g tensors.[24] The title complexes involve cobalt(II) and nickel(II) coordinated basally by four equivalent arsine oxide ligands together with axial ligation to a nitrate ion (Figure 3). The molecules crystallize in a tetragonal lattice[25] so that the polarized spectra refer to transitions with the electric-dipole vector parallel and perpendicular to the crystallographic tetrad. We address the issues of (a) whether the relative intensities observed for each chromophore can be reproduced quantitatively by the present model (and the result is affirmative), (b) whether the fits are usefully unique (and they are), (c) whether the interpretation of the "best-fit" parameter values confirms or conflicts with conclusions previously derived from the more traditional ligand-field analyses, and (d) whether the role of the $^Rt_\lambda$ parameters is more important here than hitherto and, if so, what is the significance of these parameters.

Table II. Relative[a] Values[b] of Intensity Parameters Reproducing Observed[21,22] Intensity Distributions in the Spin-Allowed Transitions of $[M(OAsPh_2Me)_4NO_3]^+NO_3^-$

	M = Co(II)		M = Ni(II)	
parameter	arsine oxide	nitrate	arsine oxide	nitrate
$^Pt_\sigma$	100[a]	0 (10)	100[a]	15 (10)
$^Ft_\sigma$	20[c]	0 (10)	20[c]	50 (15)
$^Pt_{\pi\perp}$	20 (10)	0 (10)	25 (10)	0 (10)
$^Ft_{\pi\perp}$	70 (5)	−20 (10)	85 (10)	0 (10)
$^Pt_{\pi\parallel}$	35[c]	0 (10)	35[c]	0 (10)
$^Ft_{\pi\parallel}$	0 (10)	10 (5)	0 (10)	10 (5)

	$\Delta^Rt_\lambda = {}^Rt_\lambda(AsO) - {}^Rt_\lambda(NO_3^-)$	
parameter	M = Co(II)	M = Ni(II)
Δ^Rt_σ	10 (10)	0 (10)
$\Delta^Rt_{\pi\perp}$	10 (10)	−10 (10)
$\Delta^Rt_{\pi\parallel}$	0 (5)	0 (10)

[a] Parameter values given relative to $^Pt_\sigma(AsO) = 100$ for each chromopore. [b] Estimated errors given in parentheses describe maximum increases or decreases in the given value that still reproduce experiment satisfactorily, with all other parameters held at their optimal values. [c] $^Ft_\sigma(AsO)$ and $^Pt_{\pi\parallel}(AsO)$ parameters are correlated—see text.

Analyses

Single-crystal polarized spectra of each of the cobalt(II) and nickel(II) complexes have been recorded[21,22] from crystals of different thickness at various temperatures down to 20 K. They are represented in Figure 4 together with details relating to the estimation of band intensities.

Above each abscissa are drawn long and short markers to indicate the calculated spin-allowed and spin-forbidden transitions, respectively, that were determined by the earlier ligand-field optimizations.[23] Under each spectral trace is drawn a base line with respect to which all "d–d" intensities have been determined. Those base lines are merely estimated from the likely tails of the intense charge-transfer bands lying above 25 000 cm^{-1}. Vertical lines in the figure delimit energy ranges that we use to define bands for the purposes of intensity reproduction. Thus, for example, no attempt is made to resolve the intensities of the features collected together under "band 4" of the cobalt spectra. Where resolutions have been attempted at band boundaries, these are based on the estimated spectral profiles shown as broken lines. By and large, relative intensities (obtained by cutting out and weighing copies of these adjusted spectra) are not markedly dependent on the guesses inherent in these procedures. However, a few areas of difficulty should be noted: (a) The estimate of the intensity of the spin-forbidden transition in parallel light for the cobalt complex at 18 700 cm^{-1} is necessarily uncertain. (b) The extended weak feature in parallel polarization for the same complex lying within the region of band 2 includes contributions from numerous spin-forbidden transitions as well as spin-allowed transitions. (c) The intensities of the weak features within band 1 of the nickel chromophore are difficult to estimate in the presence of the tails of the incompletely recorded bands at lower energy; however, reference to the spectral traces from much thicker crystals[21] and comparison with the spin-forbidden feature at 17 000 cm^{-1} has improved this estimate. (d) Intensity estimates for the sharp spin-forbidden feature at 13 600 cm^{-1} in the nickel system are referred to a "base line" as given by the local spin-allowed spectral trace, again as indicated by the broken lines. As absolute intensities were not reported, we refer to intensity *distributions* throughout this paper such that the sum of all observed or calculated intensities for all designated bands and for both parallel and perpendicular spectra are normalized to 100. Observed relative intensities, estimated as above, are listed in Table III.

The earlier ligand-field analyses[23] were performed first within the bases spanned by all spin-allowed free-ion terms and then within the complete d^n configuration bases. Similar procedures were adopted for the intensity analyses: for the cobalt complex, $^4P + {}^4F$ first with complete d^7 calculations later; for the nickel

(22) Gerloch, M.; Kohl, J.; Lewis, J.; Urland, W. *J. Chem. Soc. A* **1970**, 3283.
(23) Fenton, N. D.; Gerloch, M. *Inorg. Chem.* **1987**, *26*, 3273.
(24) Bencini, A.; Benelli, C.; Gatteschi, D.; Zanchini, C. *Inorg. Chem.* **1979**, *18*, 2526.
(25) Falvello, L. R.; Gerloch, M.; Raithby, P. R. *Acta Crystallogr.* **1987**, *C43*, 2029.

Table III. Comparisons between Observed[21,22] and Calculated Intensity Distributions for the Spin-Allowed Bands of $[M(OAsPh_2Me)_4NO_3]^+NO_3^-$[a]

chromophore	band interval/ $cm^{-1} \times 10^3$	relative intensities			
		∥ spectrum		⊥ spectrum	
		obsd	calcd	obsd	calcd
M = Co(II)	5.0–9.5	6	6	7	6
	9.5–15.5	8	8	14	13
	15.5–18.5	11	11	14	14
	19.2–23.0	24	25	18	18
M = Ni(II)	4.0–5.0[b]		29		15
	5.0–10.0	3	3	5	5
	10.0–16.0	12	11	18	18
	18.5–19.8	2	3	10	10
	19.8–26.9	9	9	41	41

[a] Sums of observed and corresponding calculated intensities are normalized to 100 (arbitrary units): calculated intensities with unobserved counterparts are reported on the same scale. [b] The calculated intensities for this band are included for qualitative comparison with the observed features below 5000 cm^{-1} (Figure 4). They have not been included in the fitting procedure, however, in view of the incomplete spectral traces. We note that the qualitative agreement in each case (∥ and ⊥) does not seem unreasonable.

complex, $^3P + {}^3F$ with d^8 later. Molecular absorbance tensors were calculated within the model detailed earlier[16] and summed with the symmetry-related tensors of the tetragonal lattice to yield the crystal intensities referred to herein. All computations took account of the temperatures of measurement indicated in Figure 4. The intensity parameter set comprised $^Lt_\sigma$, $^Lt_{\pi_\parallel}$ and $^Lt_{\pi_\perp}$ with $L = P$, F, and R for both arsine oxide and nitrate ligations in each complex: ∥ and ⊥ describe directions parallel and perpendicular to planes defined by either M–O–As or M–O–N, as appropriate, definitions already adopted in the earlier ligand-field analyses.[23] The intensity analyses seek to reproduce the areas of four spin-allowed band regions in each of two polarizations for each complex independently. It is therefore obvious that, a priori, we might expect extensive underdeterminacy in the present study. We recall, however, that similar—though less severe—circumstances characterized earlier intensity analyses that were, nontheless, successful.[16-18] At all stages we have looked carefully for correlations between "best-fit" parameter values. Before describing the fitting procedure, however, we note that the situation is *not* made worse by any requirement for $^Lt_{\pi\sigma}$ parameters, corresponding to locally off-diagonal $e_{\pi\sigma}$ parameters used to characterize the misdirected valency in the earlier ligand-field analyses. We show elsewhere[26] that contributions to the intensity arising from bent bonding and other forms of misdirected valency are effectively subsumed with the $\{^Lt_\lambda\}$ set ($\lambda = \sigma, \pi_\parallel, \pi_\perp$).

As discussed above, we seek to reproduce the *relative* intensities in these chromophores as the absolute magnitudes of the t parameters are inaccessible. Searches for intensity reproduction throughout parameter space were therefore implemented by fixing one parameter at 100 while others were varied in steps of 10 between +100 and −100. Several parameters were chosen in turn to be fixed at 100, so providing coverage of all parameter space. A different strategy was pursued for the $^Rt_\lambda$ parameters. Global transition moments are given by the vector sum of all local transition moments $\{q\}$ and in the case of the R terms that simply reduces[18] to the sum $\sum_i q_i^R \cos\theta_i$, where each R contribution for the local ligation is directed parallel to the bond vector inclined at angle θ_i to the global axis in question. These sums vanish identically in the global molecular symmetries of bipyramids and antiprisms.[18] There is some tendency for similar cancellation also in the present square-based pyramids. The basal ligands are oriented at about 101° to the formal molecular tetrad,[25] so that the axial contribution from the nitrate R terms will cancel those from the four basal ligands when $^Rt_\lambda(NO_3^-) \sim 0.73\,^Rt_\lambda(AsO)$. The earlier ligand-field analyses have established weaker interactions between metal and nitrate than for metal and arsine oxide; and the Ni–ONO_2 and Ni–O (arsine oxide) bond lengths are 2.01 and 2.12 Å, respectively. Although there are further differences between the axial ligations of the cobalt and nickel chromophores, which are discussed further in the next section, it was anticipated from the beginning of the intensity analyses that overall R contributions would be small and $^Rt_\lambda$ parameters would not be well-defined. The analyses were carried out, therefore, in two steps. In the first, all R contributions were ignored. Surprisingly and fortunately, an essentially unique region of $P + F$ parameter space for each chromophore provided good reproduction of the experimental intensity distributions. In the second step, the response of these regions to variations in the differences between R contributions for arsine oxide and nitrate ligations, Δ^Rt_λ, were investigated. Little correlation between the model's response to these ΔR contributions and that to P and F contributions was observed.

Overall, for each chromophore, a single, though somewhat "anisotropic", region of parameter space defined a good fit to experiment. The anisotropy for the cobalt system described a region of correlation between the $^Ft_\sigma$(AsO) and $^Pt_{\pi_\parallel}$(AsO) parameter values such that as $^Ft_\sigma$(AsO) ranged from 0 to 30, $^Pt_{\pi_\parallel}$(AsO) takes values from 100 to 10: this correlation is less extensive for the nickel system with $^Ft_\sigma$(AsO) between 15 and 25 with $^Pt_{\pi_\parallel}$(AsO) correlated between 45 and 25. All other parameter values are fairly well-defined, best-fit values being presented in Table II. Comparisons between observed and calculated intensity

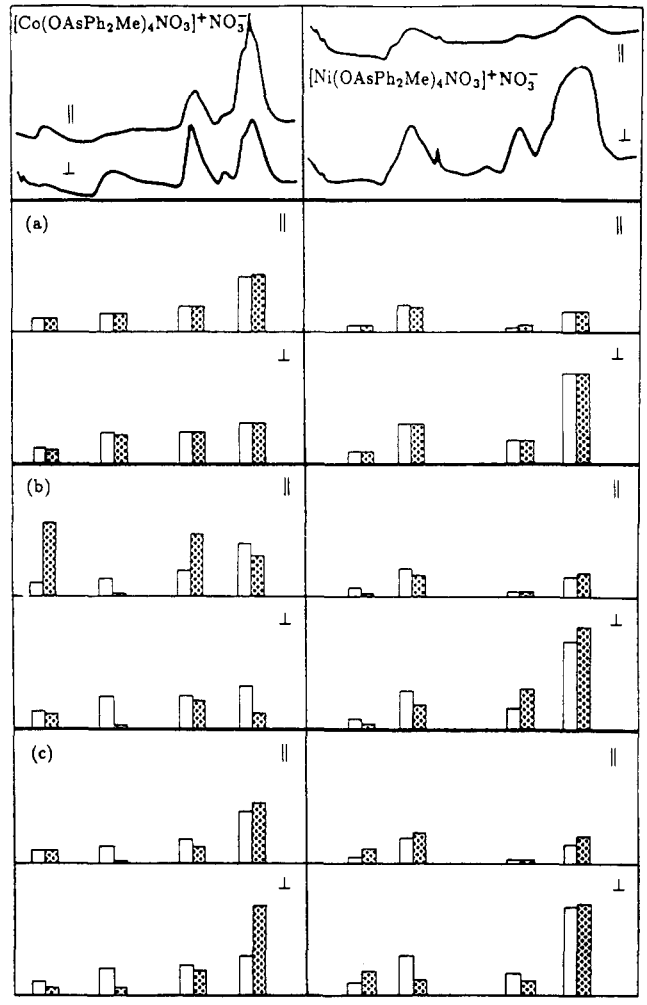

Figure 5. Comparisons between observed and calculated (dotted areas on histograms) intensities for $[M(OAsPh_2Me)_4NO_3]^+NO_3^-$ (M = Co(II), Ni(II)). Parallel and perpendicular intensities for each vertical pair of histograms are plotted on the same, arbitrary scale. Comparisons are (a) for optimal t parameter sets of Table II (for numerical comparison, see Table III), (b) for t parameter sets for nickel and cobalt complexes in Table II interchanged, and (c) for the optimal parameter sets of Table II except that $^Ft_{\pi_\perp}$(AsO) = 55 for the cobalt chromophore and 100 for the nickel.

(26) Duer, M. J.; Gerloch, M. Submitted for publication in *Inorg. Chem.*

Table IV. Calculated Relative Intensities[a] and Ligand-Field Slopes[b] for $[M(OAsPhMe)_4NO_3]^+NO_3^-$

spin multiplicity	energy/ cm^{-1}	relative intensities ⊥	relative intensities ∥	ligand-field slope/cm^{-1}	spin multiplicity	energy/ cm^{-1}	relative intensities ⊥	relative intensities ∥	ligand-field slope/cm^{-1}
				A. M = Ni(II)					
1	29977	0.005	0.03	349	1	17048	1.6	0.9	122
1	29861	0.005	0.1	354	1	15855	0.2	0.07	122
1	29423	0.003	0.03	340	1	13730	0.4	0.1	48
1	29025	0.01	0.05	340	3	12311	8.5	6.7	304
1	27695	0.01	0.07	345		12223			
1	26225	0.03	0.001	278		12102			
1	25971	0.03	0.007	310	3	11662	8.0	4.6	280
1	24490	0.16	0.03	233		11414			
3	23339	18.4	5.7	312		11364			
	23229				1	10889	0.6	0.8	−20
	23191				3	9485	1.7	1.0	283
3	22771	19.8	3.2	259		9351			
	22485					9325			
	22411				3	7965	3.3	2.1	240
1	22155	0.7	0.1	115		7900			
1	20958	2.0	0.4	298		7745			
3	19251	10.3	2.8	187					
	19165								
	19107								
				B. M = Co(II)					
2	29580	0.001	0.03	224	2	18744	1.5	0.8	10
2	29193	0.002	0.01	244	2	18407	0.7	0.5	26
2	28914	0.002	0.01	247	2	17764	0.03	0.3	15
2	28694	0.005	0.05	198	2	17418	0.1	1.2	38
2	28234	0.003	0.01	232	4	17039	4.5	5.4	111
2	27703	0.007	0.1	212		16923			
2	27665	0.005	0.02	209	2	16776	1.5	1.0	51
2	27110	0.008	0.1	202	4	16652	7.2	2.7	10
2	26818	0.001	0.02	214		16628			
2	25860	0.02	0.01	125	2	16396	0.05	0.1	7
2	24999	0.08	0.1	116	2	16090	0.2	0.04	15
2	24504	0.03	0.04	45	2	13398	0.6	1.2	−194
2	23930	0.01	0.01	70	2	12209	0.4	3.7	−198
2	23601	0.007	0.2	43	4	10521	11.3	2.5	261
2	23052	0.07	0.2	41		10560			
2	22636	0.01	0.05	29	2	10323	0.5	0.6	−260
4	20779	16.7	22.2	253	4	7497	3.4	4.7	78
	20679					7347			
2	20289	0.4	2.0	10	4	6543	2.8	1.4	107
2	19701	0.5	0.3	39		6471			

[a] Intensities on same scale as for Table III. [b] Defined as transition energy calculated with $1.05e_\lambda$ parameter values of Table V minus those values calculated with optimal parameters of Table V.

distributions are listed in Table III and shown graphically in Figure 5a. The calculated intensities in Table III for the spin-allowed transitions in each system change insignificantly on enlarging the bases from those of maximum spin-multiplicity terms only to the full d^n sets.

Calculations of the relative intensities of spin-forbidden transitions were also made within the full d^n bases. Discrete, resolved, spin-forbidden transitions are observed for the nickel complex at 13690 and 17000 cm^{-1} and for the cobalt molecule at 18700 cm^{-1}. Overall, it has proved difficult to estimate band areas associated with these transitions. However, within each set of spin-forbidden transitions, agreement between observed and calculated intensities appears to be satisfactory. Thus, both spin-forbidden features in the nickel chromophore are calculated to be more intense in perpendicular polarization than in parallel: by the ratio 6.4:1 for the sharp absorption at 13690 cm^{-1} and by the ratio 1.5:1 for the broader feature around 17000 cm^{-1}. The calculated ratio of intensities for the perpendicular spectrum for these sharp and broad transitions is 1:16 as compared with our best estimate of 1:12 from the experimental trace. In the cobalt complex, the calculated intensities of the spin doublet at 18700 cm^{-1} are in the ratio 1:1.6 for ∥:⊥ light and this too appears to agree reasonably well with experiment. On the other hand, we generally find that all comparable spin-forbidden bands are calculated to be less intense than experiment by a factor of about 30%. So the intensity distributions within the spin-forbidden transitions appear to be well reproduced, but we discern a scale factor problem between the spin-allowed and spin-forbidden subsets. We shall comment further on this feature in a future article. For the moment we note that we have observed[17] a similar quantitative scaling for spin-forbidden transitions in other systems also and believe that it represents the partial failure of an inherent assumption within the intensity model. That concerns the presumption of similar Franck–Condon factors throughout the manifold of ligand-field transitions.

Although we are unable to estimate the relative intensities of other spin-forbidden bands throughout the observed spectra, it is of interest to record their calculated values and make qualitative comparisons with experiment. Table IV lists these quantities for all transitions lying between 5000 and 30000 cm^{-1} on the same scales as those intensities given in Table III. The table also includes indicators of bandwidths computed as follows. We have considered the major determinant of bandwidths in these systems to be the changes in ligand-field strengths that accompany bond stretching. We imagine those changes to be reasonably well represented by the consequences of a totally symmetric bond stretching vibration. In the last column of Table IV, therefore, are listed the calculated energy shifts associated with replacement of the optimal e_λ set of Table V and ref 23 by one in which all diagonal e_λ values are increased by 5%. We therefore enquire how well these computed slopes of transition energies correlate with observed bandwidths.

Table V. Summary of e Parameters (cm^{-1}) Affording Optimal Reproduction[23] of Crystal Paramagnetic Susceptibilities, Molecular g^2 Tensors (for the Cobalt Complex), and d–d Transition Energies in $[M(OAsPh_2Me)_4NO_3]^+NO_3^-$

CLF parameter	M = Co(II)		M = Ni(II)	
	arsine oxide	nitrate	arsine oxide	nitrate
e_σ	3500	100	3550	1700
$e_{\pi_\perp}$	980	−200	950	100
$e_{\pi_\parallel}$	875	650	675	350
$e_{\pi\sigma}$	945	950	880	1650

Consider, first, all these data for the nickel chromophore. Calculated "bandwidths" for the spin-allowed bands 2 and 4 (Figure 4) are similar and considerably greater than for band 3, in good qualitative agreement with experiment. The broad trace for band 1 suggests that the calculated "bandwidth" fits well also. The sharpness of the spin-forbidden transition at 13 730 cm^{-1} is well reproduced as is also the rather broader profile of that at ca. 17 000 cm^{-1}: compare also the width of this spin-forbidden band with that of the spin-allowed band (band 3) at ca. 19 000 cm^{-1}. Then consider the calculated relative intensities of the spin-forbidden transitions. In addition to those discussed earlier and corresponding to ones observed as quite well resolved, we note the relative significance of the transition at 20 958 cm^{-1}, which appears to be responsible for the shoulder on the large spin-allowed band 4 in both perpendicular and parallel polarization. Similarly, the spectral traces appear to show the presence of the spin-forbidden transitions at 10 889 cm^{-1}, particularly in parallel light. Finally, we observe that the calculated intensities of all spin-singlet transitions lying above 24 000 cm^{-1} (and generally well removed from all spin-allowed bands) are very small indeed, again in agreement with their nonappearance in the experimental traces.

For the cobalt complex, agreement between observed bandwidths of the spin-allowed bands and corresponding calculated ligand-field shifts is fair, if not dramatic. The narrowest such band is band 3 from both experiment and calculation. The appearance of the spin-forbidden feature at ca. 18 800 cm^{-1} seems due to the three narrow and intense (relative to other spin-doublets) doublets at 18 407, 18 744, and 19 701 cm^{-1}. Then, the pronounced shoulder on the low energy side of spin-allowed band 4, particularly in parallel light, is again qualitatively reproduced by the narrow and significantly intense feature calculated at 20 289 cm^{-1}. Of particular interest are the intensities of the spin doublet at 12 209 cm^{-1} and spin quartet at ca. 10 500 cm^{-1}. In perpendicularly polarized light, the quartet predominates, but in parallel light, it is the doublet that is the larger feature: again, this seems to agree with experiment rather well. Finally, as for the nickel complex, all spin-forbidden transitions beyond the energy region of the quartets have very small calculated intensities. Those at ca. 23 000 cm^{-1} have been observed, by using a very thick crystal,[22] as very weak features indeed. Note that the small features in perpendicular polarization of both cobalt and nickel complexes at ca. 28 000 cm^{-1} are not assigned[21,22] as "d–d" transitions.

Overall, therefore, detailed predictions from the whole model with respect to relative bandwidths and band intensities that were not part of the analytical process per se seem to correlate with experiment remarkably well. We shall report later on further estimates of bandwidths in other systems.

Returning to the spin-allowed bands that form the basis of the present intensity analysis, we have also performed a number of calculations to illustrate the sensitivity of quoted best fits. First, we exchanged intensity parameter sets between the two chromophores, keeping all else the same. The calculated intensity distributions so produced are shown in Figure 5b. That for the nickel chromophore is obviously poorer than that calculated with the optimal parameter set (and Figure 5a), though not grossly unsatisfactory. On the other hand, that for the cobalt complex is quite unacceptable. Second, to illustrate our estimated tolerances on the reported t parameters, we show in Figure 5c the much poorer quality of reproduction obtained when the $^Ft_{\pi_\perp}$(AsO) values of Table II are replaced by the values 55 or 100. Finally, we note that interchange of $^Pt_\lambda$ and $^Ft_\lambda$ values throughout the parameter sets (where they are different) yields totally unacceptable reproduction of the observed spectral distributions.

Discussion

A. Number of Parameters. This new model[16] for the calculation of ligand-field intensity distributions is highly parametrized. From the outset it is important to dispel any disbelief and rejection that too commonly accompany such schemes.

First, we are obliged to accept a parametric approach anyway, as the calculation of absolute intensities, ab initio, is a task of enormous proportions in this area of chemistry, given the well-established difficulty of accurately computing even ligand-field energies. We have behind us now a very long and invariably successful record for conventional ligand-field analysis of transition energies and magnetism in terms of local or cellular parametrization, so it was natural to develop an analogous approach for the study of "d–d" intensities. As outlined in the Introduction and introduced in full elsewhere,[16] the $\{^Lt_\lambda\}$ parameters merely set out the degrees of freedom that follow inevitably from that position. In short, the t parameters properly reflect all physical features in these chromophores that cannot be fixed otherwise, by symmetry or reasonable approximation: the structure is well based.

Second, we note that, despite the much larger number of parameters than spectral intensities, good reproductions of the observed data have been obtained in essentially *unique* volumes of parameter space for each chromophore. An acceptance of this irrefutable empirical observation must be made alongside a recognition of the nonlinearity of the model. That most regions of t parameter space are unable to support any acceptable reproduction of the experimental intensity distributions must, in part, reflect the constraints within both the eigenvalues and eigenfunctions that were provided by prior ligand-field analysis. Our experience to date, both published[17,18] and current, is that analyses with the present highly parametrized intensity model *are* tractable and generally lead to essentially unique discriptions of the underlying bonding structure.

Third, as described in the preceding section, the number of $^Rt_\lambda$ parameters is effectively halved so that the apparent underdeterminacy suggested at the beginning is rather less severe. The largest uncertainty remaining is the correlation found, for each complex, between $^Ft_\sigma$(AsO) and $^Pt_{\pi_\parallel}$(AsO) parameter values. This is borne in mind in what follows, but the semiquantitative nature of our final conclusions is unaffected by it.

B. Significance of the *t* Parameters. Our interpretation of the intensity parameter values in Table II is made in the light of the ligand fields defined earlier[23] by the e parameters and with reference to theoretical and empirical conclusions drawn from the seminal studies of this intensity model.[16-18] We review and develop these latter first.

Of particular concern is the significance of the left superscript labels of the $^Lt_\lambda$ parameters, for while the descriptions $\lambda = \sigma$, π_x, and π_y are familiar enough, the subdivision $L = P$, F, and R has received little exposure. Consider the P and F contributions and refer to the equations in the Introduction. The magnitudes of $^Pt_\lambda$ and $^Ft_\lambda$ parameters depend upon the integrals $\langle d|er|p\rangle$ and $\langle d|er|f\rangle$, and also upon the coefficients b_p and b_f. In part, these coefficients relate to the contribution of metal p (and, surely negligible, f) functions within the bond orbitals of (1), but mostly to contributions of ligand orbitals, which, via the expansion in (2), appear as metal-centered p and f functions. While metal 3d–4p mixing in a crystal-field model is known[27] to be trivial, d–p mixing within a covalent picture (arising from the simultaneous overlap of ligand functions with both metal d and p orbitals) acquires significance. We expect such metal d–p mixing to be larger for metal–ligand σ bonding than for π bonding. So, while these contributions to the intensty parameters will surely be much less important than those arising from the multipole expansions of the original ligand functions, they should be such as to augment ^Pt parameters over ^Ft more for σ bonding than for π bonding.

(27) Ballhausen, C. J.; Liehr, A. D. *J. Mol. Spectrosc.* **1958**, *2*, 342.

In the main, however, the chemical significance of ${}^{P}t_{\lambda}$ and ${}^{F}t_{\lambda}$ parameter values is to be discovered from an investigation of the multipole expansion in (2). This is done with respect to three qualities of a metal–ligand bond: (a) bond length; (b) bond symmetry, that is, σ versus π; (c) the electron distribution within the bond.

Bond Length. Increasing separation of metal and ligand will be accompanied by decreasing metal–ligand mixing, smaller c coefficients in (1), and hence decreasing magnitudes of both ${}^{P}t_{\lambda}$ and ${}^{F}t_{\lambda}$ parameters. Further, insofar that a two-center, multipole expansion reconstructs more distant ligand functions with increasing proportions of higher order multipoles, bond lengthening is expected to diminish contributions to ${}^{P}t_{\lambda}$ parameters more rapidly than to ${}^{F}t_{\lambda}$. Taking both points together, longer bonds will be reflected in decreasing ${}^{L}t_{\lambda}$ parameters ($L = P, F$) and decreasing ${}^{P}t_{\lambda}:{}^{F}t_{\lambda}$ ratios. To some extent, however, these trends will be attenuated by the nature of the electric dipole operator, $e\mathbf{r}$, appearing in the integrals $\langle \mathrm{d}|e\mathbf{r}|\mathrm{p}\rangle$ and $\langle \mathrm{d}|e\mathbf{r}|\mathrm{f}\rangle$. That operator increases linearly with distance from the metal origin and so contributions from these integrals will tend to be greater from the more distant parts of the bond. However, as the expansion functions p and f become more diffuse with increasing bond length, it is difficult to guess the overall result from this factor. It is the case, however, that calculations reported[18] in Part III of the original papers on this model, calculations that include variations of both integral and expansion coefficients of (3) together, support the qualitative trends summarized above.

Bond Symmetry. It is commonplace to observe ligand-field e_{π} parameters taking magnitudes rather smaller than e_{σ}: ratios for $e_{\pi}:e_{\sigma}$ are often around 0.1–0.4. Yet the first studies of the present intensity model, since confirmed by further work in preparation, often yielded t_{π} values that are comparable with t_{σ}. As discussed further below, similar trends are evident for the t values of Table II in the present study. Some qualitative understanding of this difference emerges from consideration of the functional forms of the two types of parameter. The CLF e_{λ} parameters ($\lambda = \sigma, \pi_x, \pi_y$) are dominated by the so-called "dynamic" contribution[1-3]

$$e_{\lambda} \sim |\langle \mathrm{d}_{\lambda}|v^{l}|\chi_{\lambda}\rangle|^{2}/(\epsilon_{\mathrm{d}} - \bar{\epsilon}_{\chi}) \qquad (10)$$

in which $\bar{\epsilon}_{\chi}$ and ϵ_{d} are the energies of the bond orbital χ and of the mean d orbitals, respectively. The operator v^{l} in the numerator is that part of the local effective ligand field that does not ultimately contribute to the spherical molecular ligand field. It arises from all "nonspherical" (again, meaning noncontributory to the molecular mean potential) electron density within the local cell, and it transforms totally symmetrically within that cell. This last point means that the magnitudes of all e_{λ} (σ and π) are affected by the same overall bond electron density, albeit unequally. That e_{π}, for example, is nonzero in any particular case arises from the presence of a χ_{π} orbital in the numerator in (10). Contributions to the integral in (10) are greatest in those regions of space in which the product of the functions d, v^{l}, and χ_{λ} together is greatest, of course. When $\lambda = \pi$, the magnitude of e_{λ} is generally less than when $\lambda = \sigma$, for there is less π-bond density expected than σ-bond density. So while the denominator of (10) may well be less for $\lambda = \pi$ than for $\lambda = \sigma$, we still see smaller e_{π} values than e_{σ} values, essentially because of the much smaller concentration of electron density in the π-bonding regions.

Lesser π overlap between metal and ligand than σ overlap, and hence smaller c coefficients in (1) and b coefficients in (4), (7), and (8), similarly implies smaller magnitudes for t_{π} than for t_{σ} parameters. On the other hand, that same lesser overlap is associated with less electron donation from ligand to metal (other factors being equal, of course) so that the χ in (4) tends to be concentrated more on the ligand for π interactions while being shared more with the metal for σ interactions. Since the electric dipole operator emphasizes the more distant parts of the cellular space, the relatively larger concentration of bond orbital nearer the ligand is reflected in larger contributions to the t_{π} parameters. So, while many, intimately related, trends must occur together in given real systems, the larger $t_{\pi}:t_{\sigma}$ ratios often observed, relative to $e_{\pi}:e_{\sigma}$, are to be seen against the difference between the operators v^{l} and $e\mathbf{r}$. The ligand-field operator v^{l} maximizes where most bond density ($\sigma + \pi$) maximizes; $e\mathbf{r}$ emphasizes the more distant regions.

This discussion has thus far addressed the relative magnitudes of t_{π} and e_{π} parameters. We look now at the role of local symmetry upon $t_{\pi}:t_{\sigma}$ ratios. In particular, we review the nature of the sort of two-center expansion summarized in (3). No generality is lost by consideration of the form of multipole expansion described by Sharma,[20] in which a ligand function is expanded in terms of *one* metal-centered s orbital, *one* p orbital, *one* d orbital, etc. In this form, both the coefficients of the different multipoles and the radial characters of those basis functions are varied to implement the expansion. We can discern trends in $t_{\pi}:t_{\sigma}$ ratios against this background. In the case of σ bonding, a more distant ligand function is reproduced, not only by increasing contributions from higher order multipoles, but also by more expanded radial properties of those multipoles. So far as this latter effect alone is concerned, one need not expect any dramatic change in the ratio $\langle \mathrm{d}|e\mathbf{r}|\mathrm{p}\rangle:\langle \mathrm{d}|e\mathbf{r}|\mathrm{f}\rangle$, though there will be some. The main effect upon ${}^{P}t_{\sigma}:{}^{F}t_{\sigma}$ ratios will arise, as discussed above, from the changing proportions of p and f multipoles in the expansion. The situation is rather different in the case of π orbital expansion, however. Greater metal–ligand separation in this case is reproduced very poorly by expansion of the radial properties of the multipole expansion functions, for otherwise an unwanted lateral expansion of the orbital would accompany bond stretching. Instead, longer bonds give rise almost exclusively to higher order multipoles of essentially unchanged radial character. In consequence, we expect, other things being equal as ever, that increasing bond lengths will increase the $F:P$ ratio of t_{π} parameters much more rapidly than that of t_{σ} parameters. Once more, numerical calculations of ${}^{P,F}t_{\lambda}$ parameters for idealized descriptions of metal and ligand have confirmed these qualitative predictions (see Figure 5 of ref 18).

Electron Distribution in the Bonds. Trends in $P:F$ ratios are to be expected in response to changing polarization and bulk of bond orbitals. The description of local ligand-field orbitals in (4) as mean metal d plus "the rest" recognizes implicitly all that has taken place on bond formation. These orbitals—and, hence, both ligand-field and intensity parameters that monitor them—probe those changes. Qualitatively at least, increasing polarization of bond orbitals towards the metal is expected to affect t parameters somewhat like bond shortening, so that these two variables might be considered[18] together in terms of the "effective bond length". Increasing polarization of electron density toward the metal along some related series of metal–ligand bonds is thus expected to be monitored in spectral intensities by increasing ratios ${}^{P}t_{\lambda}:{}^{F}t_{\lambda}$.

We may also consider what changes in such ratios would accompany alterations in the lateral extent of metal–ligand bonds. Consider the case of a series in which the lateral bulk of a given bond increases while all else, including bond length, stays constant. Such a variation would be reproduced within the multipole expansion above by a greater diffuseness (enlargement) of the radial coefficients in the expansion, coupled with a diminishing role of higher order multipoles so as to cancel this effect parallel to the bond vector. As before, changes in $\langle \mathrm{d}|e\mathbf{r}|\mathrm{p}\rangle$ and $\langle \mathrm{d}|e\mathbf{r}|\mathrm{f}\rangle$ integrals in response to increased diffuseness of the p and f functions are likely to be broadly similar and so the dominant factor here is the changing proportion of p and f functions in the two-center expansion. Overall, therefore, we expect "fatter" bonds to favor larger ${}^{P}t_{\lambda}:{}^{F}t_{\lambda}$ than "thinner" ones, as usual, other factors being equal.

Summary of Trends. The conclusions of the preceding three subsections in brief are then (a) that increasing bond length and/or bond polarization toward the ligand should decrease the magnitudes of the ${}^{L}t_{\lambda}$ and increase the ratio ${}^{F}t_{\lambda}:{}^{P}t_{\lambda}$, (b) that this increasing $F:P$ ratio should be more marked for $\lambda = \pi$ than for $\lambda = \sigma$, and (c) that increases in the lateral spread of bond orbitals (fatter bonds) should result in decreasing $F:P$ ratios. These guiding principles are now exploited in interpretations of the analytical results of the title chromophores.

C. Comparisons between the Ligand-Field and Intensity Parameters for $[M(OAsPh_2Me)_4(NO_3)]^{+}NO_3^{-}$ ($M = Co^{II}, Ni^{II}$). In Table V are listed the e parameter values for the complexes in

this study as determined by the earlier ligand-field analysis.[23] Two features characterize the ligand fields in these systems: aspects of misdirected valency with both arsine oxide and nitrate ligations and the very different $e_\sigma(NO_3^-)$ values for the cobalt and nickel complexes. These latter are to be understood in terms of the steric role of the d_{xy} orbital, which is doubly filled in the nickel complex but only singly filled in the cobalt complex. Bond tightening that is to be expected with increasing effective nuclear charge on replacing cobalt by nickel is frustrated for the basal coordination by the extra d_{xy} electron and must be compensated for by a decreased bond length and increased ligand field of the nickel–nitrate ligation. In both chromophores, the low value of $e_\sigma(NO_3^-)$ also reflects the negative ligand-field contribution of the coordination void opposite.

The t parameter values of Table II accord with these ligand-field descriptions remarkably well. First, notwithstanding the quite different spectra and d^n configurations of the cobalt and nickel chromophores, the optimal t parameter values for the arsine oxide ligations describe essentially the same pattern: the e parameter sets for the two metal–arsine oxide interactions show the same consistency. The typically short M–OAs bonds (2.01 Å) with the oxygen donor atom are characterized by a ${}^Pt_\sigma$ parameter that dominates over ${}^Ft_\sigma$. That ${}^Ft_{\pi_\perp}$ is greater than ${}^Pt_{\pi_\perp}$ for the present metal–arsine oxide coordinations is to be understood, as discussed above, in terms of the various tendencies for t_π parameters to be dominated by the F contribution more easily than for t_σ. One presumes that the only modest π-donor roles of the arsine oxides are insufficient to override this tendency. What then of the significant (albeit not well-defined, in view of the correlation described in the analysis) positive value for ${}^Pt_{\pi_\parallel}$ as compared with the zero value for ${}^Ft_{\sigma_\perp}$? This result appears to be a splendid confirmation of the misdirected valency[28-30] determined by the earlier ligand-field analysis. In that study,[23] the significant value of the local off-diagonal ligand-field parameter $e_{\pi\sigma}$ was argued to reflect the role of the nonbonding lone pair of electrons on the donor oxygen atom. The nonzero value of $e_{\pi_\parallel}$ arises from the same source. Elsewhere,[26] we show how extra $t_{\pi\sigma}$ parameters are not required in the internsity model—essentially because the local transition-moment matrix is not diagonal anyway—but that extra "σ–π" mixing which arises by any form of misdirected valence will be taken up in modified t_σ and $t_{\pi_\parallel}$ parameters (assuming $\parallel$ means, as here, parallel to the plane of misdirected valence). In effect, therefore, the ${}^Lt_{\pi_\parallel}$ parameters for the present metal–arsine oxide ligations represent some part of the corresponding ${}^Lt_\sigma$ parameters admixed by the misdirected nature of the local metal–ligand bonding. As the t_σ parameters are dominated by the P contribution, so also are the $t_{\pi_\parallel}$ parameters.

Consider now the t parameter values characterizing the metal–nitrate ligations. The earlier ligand-field analyses provided a view of weak bonding in the nickel complex (the nickel–nitrate bond length is 2.12 Å)[25] but weaker bonding still in the cobalt molecule: $e_\sigma(Co–NO_3) - e_\sigma(Ni–NO_3) = 1600\ cm^{-1}$. The present intensity analyses clearly reflect that difference. While a significant contribution to the spectral intensity distribution arises from the nickel–nitrate coordination, rather little derives from the cobalt–nitrate interaction. Furthermore, ${}^Ft_\sigma > {}^Pt_\sigma$ for the $Ni–NO_3$ ligation, in contrast with the situation for the metal–arsine oxide complexes, presumably reflecting the much longer metal–oxygen distance in this case. As for the basal ligands, the metal–nitrate interaction is also characterized by misdirected valence, though here it arises mostly through simple bent bonding. Once more, we observe the relative magnitudes of the ${}^Lt_{\pi_\perp}$ parameters taking on the relative contributions of the ${}^Lt_\sigma$ parameters. With rather less confidence in view of their small values in relation to estimated errors, we can finally offer some commentary on the ${}^Ft_\pi$ parameters for the $Co–NO_3$ ligation. First, we observe that the $e_{\pi_\perp}$ value for this interaction is uniquely negative and so is the ${}^Ft_{\pi_\perp}$ parameter. Then we recall that, because of the negative contributions to e_σ(void) in these systems, the very low values of $e_\sigma(NO_3^-)$ represent the averages of nitrate and void contributions. So, even in the cobalt complex, the ligand-field strength of the nitrate is not negligible. However, at the rather long distance of ligation here, we expect that $\pi_\perp$ electron density is essentially concentrated on the ligand. As the electric dipole operator emphasizes more distance regions, provided, of course, that some π overlap still remains, the numerically larger values for ${}^Ft_{\pi_\perp}$ relative to ${}^Lt_\sigma$ can be understood. And further, it is the F component that predominates over the P, as expected for "long-distance" contributions. Overall, however, it must be recognized that we have reached the limits of reliability for these small t parameter values in the present analysis.

Finally, it is just possible to discern a significant pattern in the differences between the ${}^Rt_\lambda$ parameters of the arsine oxide and nitrate ligations in the two chromopores. As discussed in the Analysis section, intensity contributions from axial and basal ligands tend to cancel. Within the error estimates of Table II, such appears to be the case for the nickel complex. On the other hand, a significantly lesser contribution from the cobalt nitrate ligation seems to be evident from the small positive Δ^Rt_λ values there. Qualitatively, at least, the R contributions determined (albeit rather approximately) by the present analysis, concur with the P and F parameter values in reflecting the weaker nitrate coordination in the cobalt chromophore.

Summary

The intensity distributions within the "d–d" spectral transitions of the title complexes have been reproduced quantitatively by this new approach. The model sets the calculation of such spectral intensities within the broader structure of ligand-field theory so that these properties are to be considered as experimental data on a par with other ligand-field properties like paramagnetism or ESR g values. The parametric structure of the model is such as to separate those quantities relating to ligand position and orientation from those relating to features of local σ or π bonding and from those reflecting quantitative aspects of electron density distribution in the bonds. Chemical principles that enable discussion of broader chemical qualities as well as of traditional ligand fields serve equally well to provide the basis of the interpretation of the present intensity parameters. Values for these parameters have been determined here nearly uniquely, despite the high degree of parametrization, and certainly uniquely enough to establish a view of the electron distribution within the metal–ligand bonds that accords in vitually every detail with that deriving from the earlier traditional ligand-field analyses. Even with the limited experience with this new model to date, it appears that confidence may be placed in its results to the same level of detail that characterizes modern ligand-field analysis of transition energies and magnetism.

Acknowledgment. We thank Dr. Melinda Duer for many useful discussions and acknowledge the financial support of the SERC for a Research Studentship to N.D.F.

(28) Deeth, R. J.; Duer, M. J.; Gerloch, M. *Inorg. Chem.* **1987**, *26*, 2573.
(29) Deeth, R. J.; Duer, M. J.; Gerloch, M. *Inorg. Chem.* **1987**, *26*, 2578.
(30) Deeth, R. J.; Gerloch, M. *Inorg. Chem.* **1987**, *26*, 2582.